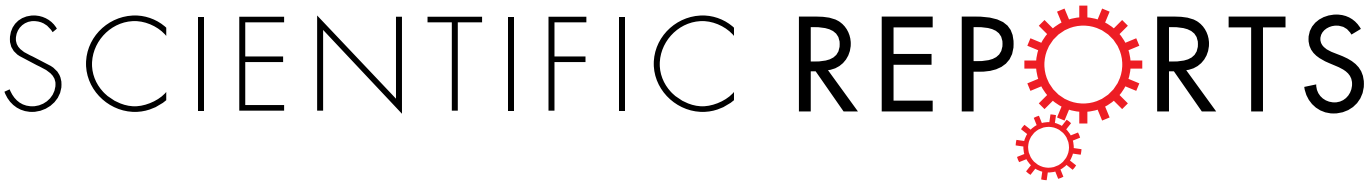

OPEN

Mixed Molybdenum Oxides with Superior Performances as an Advanced Anode Material for Lithium-Ion Batteries

Received: 10 August 2016
Accepted: 13 February 2017
Published: 15 March 2017

Di Wu[1,*], Rui Shen[1,*], Rong Yang[1], Wenxu Ji[1], Meng Jiang[2], Weiping Ding[1] & Luming Peng[1]

A simple and effective carbon-free strategy is carried out to prepare mixed molybdenum oxides as an advanced anode material for lithium-ion batteries. The new material shows a high specific capacity up to 930.6 mAh·g^{-1}, long cycle-life (>200 cycles) and high rate capability. 1D and 2D solid-state NMR, as well as XRD data on lithiated sample (after discharge) show that the material is associated with both insertion/extraction and conversion reaction mechanisms for lithium storage. The well mixed molybdenum oxides at the microscale and the involvement of both mechanisms are considered as the key to the better electrochemical properties. The strategy can be applied to other transition metal oxides to enhance their performance as electrode materials.

As one of the solutions for our new energy-based economy, lithium ion batteries are widely used in mobile devices, such as cellular phones and laptops, because of their relatively high volumetric and gravimetric energy density[1,2]. However, in order to meet the requirements for applications in electric vehicles, safe electrode materials with less cost, higher energy density, better rate performance and longer service life need to be designed[3]. Transition-metal oxides, which often have much higher theoretical capacity than traditional graphite materials, have been extensively studied as the anode materials for lithium ion batteries[4]. Molybdenum oxides (including both MoO_2 and MoO_3) represent attractive candidates due to their high theoretical capacity (about 838 mAh·g^{-1} for dioxides and 1117 mAh·g^{-1} for trioxides). Bulk molybdenum oxides, however, show much lower capacities compared with their theoretical ones, which can be attributed to the significant volume change during the charge and discharge processes and the intrinsic slow kinetics for the conversion reactions[5].

Recently, metal oxide nanostructures, especially nanostructured oxides have been prepared as anode materials for lithium ion batteries due to their short diffusion length, larger reaction surface area between the electrode and electrolyte, as well as extra space for better accommodation of the strain induced by large volume changes[6–11]. For example, molybdenum dioxide with a yolk-shell structure achieves a discharge capacity of 847.5 mAh·g^{-1} after 50 cycles at 50 mA·g^{-1} [12]. Uniform carbon coated nanospheres exhibit a discharge capacity of 410 mAh·g^{-1} after 30 cycles even at 3 C rate[6]. Coating highly conductive materials, such as carbon, is another strategy to improve the performances of metal oxides by increasing the electrode conductivity, as well as possibly improving the surface chemistry of the active material. The MoO_2 hollow structures coated with Mo_2N show a capacity of 815 mAh·g^{-1} after 100 cycles at 100 mA·g^{-1} [13]. Nevertheless, it is usually expensive to prepare the complex nanostructure and the capacity fading often occurs during the cycling process, while coating conductive materials with low capacity reduces the specific capacity of the active materials.

Partial oxidation or reduction strategy has been employed to improve the electrochemical properties of cathode materials, for example, controlled reduction of LiV_3O_8 generate $Li_xV_2O_5/LiV_3O_8$ composite with significantly improved cycling performancs and rate capability[14]. Herein we report a very simple and convenient method to prepare the mixed molybdenum oxides (MMO, MoO_x, $2 < x < 3$) by moderately oxidizing molybdenum dioxide nanoparticles under mild oxidizing atmosphere. The obtained MMO exhibits a discharge capacity as high as 930.6 mAh·g^{-1} at a current density of 200 mA·g^{-1} after 200 cycles as an advanced material, indicating this material has potential for applications in lithium-ion batteries.

[1]Key Laboratory of Mesoscopic Chemistry of MOE and Collaborative Innovation Center of Chemistry for Life Sciences, School of Chemistry and Chemical Engineering, Nanjing University, Nanjing 210093, China. [2]General Motors R&D, Warren, MI 48090, USA. *These authors contributed equally to this work. Correspondence and requests for materials should be addressed to W.D. (email: dingwp@nju.edu.cn) or L.P. (email: luming@nju.edu.cn)

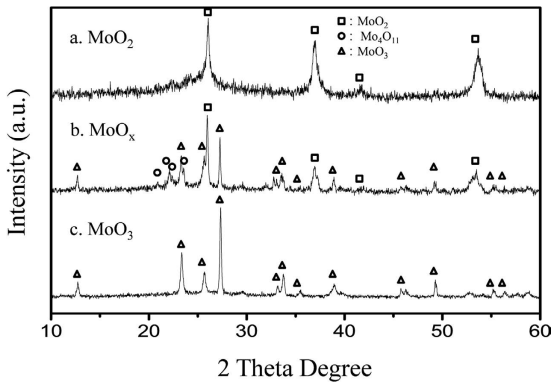

Figure 1. XRD patterns of the MoO_2 nanoparticles annealed in N_2 flow with different O_2 content ((**a**), 0%; (**b**), 0.2%; (**c**), 1% O_2 in N_2).

Experimental Section

Preparation of the MoO_2 nanoparticles. MoO_2 nanoparticles were prepared by using a hydrothermal method reported by Liu *et al.*[15]. In a typical experiment, 1 g of ammonium heptamolybdate tetrahydrate was dissolved into the mixed solvent of 45 mL distilled water and 5 mL ethylene glycol (EG). After that, the mixture was transferred into a 100 mL Teflon-lined stainless-steel autoclave and was kept in an oven at a temperature of 180 °C for 48 h. The resulted black precipitate was centrifuged, and then washed by distilled water and followed by ethanol for three times. The product was finally dried at the 80 °C.

Preparation of the MMO and MoO_3 nanoparticles. To prepare MMO, the as prepared MoO_2 nanostructured powders was heated in a tube furnace at a rate of 5 °C·min^{-1} to 500 °C and kept at the temperature for 100 min. A mixed gas containing a small fraction of oxygen in nitrogen was flowed into the system during heating at a rate of 20 mL/min. The fractions of oxygen were controlled as 0.2% and 1%, in order to achieve the final product MMO and MoO_3, respectively.

Materials Characterization. The XRD patterns were acquired with an X-ray diffractometer (Philips Analytical X'pert Pro) at a 2θ range of 10–70°. The diffractometer was equipped with a Cu Kα radiation (λ = 1.5418 Å) and operated at 40 kV and 40 mA. The air sensitive samples were protected by Kapton films in the XRD measurement. The morphology of the samples were investigated using a field-emission scanning electron microscope (Hitachi FE-SEM S4800). X-ray photoelectron spectroscopy (XPS) was used to survey the surface compositions and the chemical states of the samples (PHI5000 VersaProbe, PerkinElmer). The hydrocarbon C 1 s peak at 284.5 eV was chosen as the reference for the binding energies. The XPS spectra were analyzed with the software XPSPeak 4.1. The ratio of the peak area of the Mo $3d_{5/2}$ peak to the Mo $3d_{3/2}$ peak is fixed to 1.5 while the binding energy separation is set to 3.0 eV. A Bruker Advance III 400 MHz spectrometer with a 3.2 mm Magic Angle Spinning (MAS) probe was used for acquiring the ^{7}Li solid-state NMR spectra at a resonant frequency of 155.46 MHz. A spin-echo and a 2D exchanged pulse sequence were used in the data acquisition. In order to select reduce the intensity of the resonance due to the SEI, a T_2 filter was used in the spin-echo NMR data acquisition. After discharging to 5×10^{-3} V, the self-supported electrode[16] was taken out, rinsed with dimethyl carbonate (DMC) to remove the residual electrolyte, before it was dried and packed into NMR rotors in an Ar glove box, and spun at 18 or 20 kHz for NMR data collection. A 1 M LiCl aqueous solution was used to set the spectral reference to 0 ppm.

Electrochemical Characterization. Electrochemical measurements were performed on coin cells (model 2032) with lithium metal foils as the reference and counter electrodes at ambient temperature. 70 wt% of as prepared samples, 20 wt% acetylene black (conducting additive), and 10 wt% polyvinylidene fluoride (binder) were blended with N-Methyl-2-pyrrolidone (NMP) to make a slurry and then spread onto a copper foil current collector. After drying at 80 °C for 6 hours, the electrode was punched and then dried under vacuum at 120 °C for 12 hours. The electrodes were then transferred to an argon-filled glove box where both the moisture and oxygen concentrations were kept below 1 ppm. The electrolyte was prepared by dissolving 1 M $LiPF_6$ in a mixture of ethyl methyl carbonate (EMC), ethylene carbonate (EC) and dimethyl carbonate (DMC) (1:1:1 in weight) solution while a Celgard 2325 film was used as the separator. An electrochemical station (CHI660D) was used to obtain cyclic voltammetry (CV) at ambient temperature. CV measurements were performed over a potential range of 5×10^{-3}–3.0 V (vs. Li^+/Li) at a scan rate of 2×10^{-4} V s^{-1}. Galvanostatic discharge–charge measurements were performed at different rate on a battery testing system (LAND CT2001A model, Wuhan Jinnuo Electronics Co. Ltd) with a voltage window range from 5×10^{-3} to 3.0 V (vs. Li^+/Li).

Results and Discussion

The XRD patterns of different molybdenum oxide nanoparticle samples are shown in Fig. 1. All of the XRD peaks for MoO_2 nanoparticles annealed with pure N_2 can be indexed to MoO_2 (Fig. 1a, ICSD:080830), while the sample heated with a high concentration of O_2 (1% O_2 in N_2) in the flow is completely oxidized to MoO_3 (Fig. 1c,

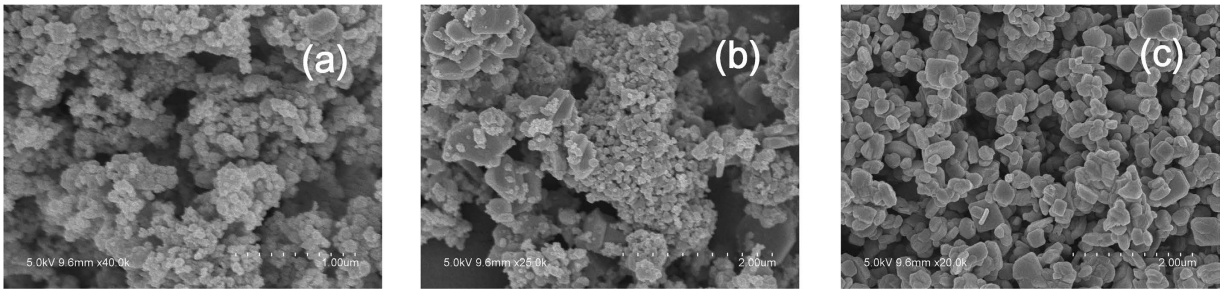

Figure 2. SEM images of MoO_2 (**a**), MMO (**b**) and MoO_3 (**c**).

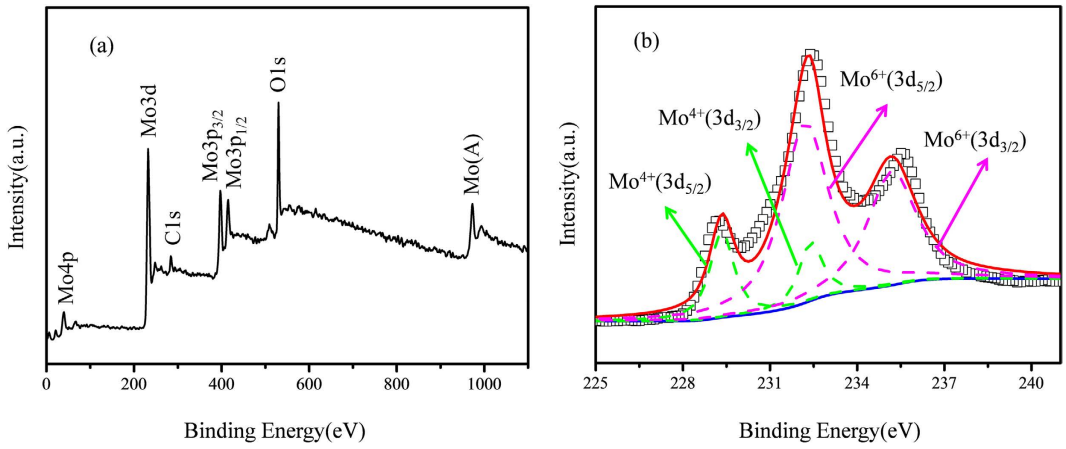

Figure 3. XPS patterns of MMO: (**a**) survey spectrum and (**b**) high-resolution Mo 3d region.

Peak	Position (eV)	Relative Peak Area (%)	FWHM (eV)
Mo^{4+} ($3d_{5/2}$)	229.3	12.0	1.0
Mo^{4+} ($3d_{3/2}$)	232.4	8.0	1.0
Mo^{6+} ($3d_{5/2}$)	232.2	48.0	1.9
Mo^{6+} ($3d_{3/2}$)	235.2	32.0	2.0

Table 1. Results of peak fitting for MMO in the Mo 3d region.

ICSD:076365)[17]. However, MoO_2 nanoparticles treated with a smaller fraction of O_2 (0.2% O_2 in N_2) show mixed phases which can be attributed to MoO_2, MoO_3, as well as a small fraction of Mo_4O_{11} (Fig. 1b, ICSD:089340), indicating the nanoparticles have been partially oxidized, noted as MMO. By using the Scherrer equation, the mean diameters of MoO_2 and MoO_3 nanocrystallites can be determined as 5–8 and 50 nm, respectively, while the average size of MMO is in between.

Figure 2 shows the SEM images of the obtained MoO_2, MMO and MoO_3 samples. Small agglomerates with a diameter of about 50 nm composed of smaller and round shaped nanoparticles can be observed for the MoO_2 sample, while MoO_3 are much larger in size (100 to 500 nm). The SEM image of MMO shows this sample is composed of small particles with different sizes, resembling a mixture of the above two materials. The results indicate that MMO are not uniformly oxidized, in agreement with the XRD data.

X-ray photoelectron spectroscopy (XPS) measurement was performed in order to investigate the surface valence states of Mo in MMO, and the results are shown in Fig. 3. The peaks of Mo 3d and O 1 s can be observed in the survey spectra (Fig. 3a), and the former was further examined. The two peaks at about 232.0 and 235.0 eV are characteristic of Mo^{6+}, and can be attributed to Mo^{6+} ($3d_{5/2}$) and Mo^{6+} ($3d_{3/2}$), respectively[18]. The lower energy peak centered at 229.3 eV can be attributed to Mo^{4+} ($3d_{5/2}$), suggesting that the Mo ions on the surface of MMO are in mixed valence states[19]. The spectrum was fitted into two doublets ascribed to Mo^{6+} ($3d_{5/2}$)/Mo^{6+} ($3d_{3/2}$) and Mo^{4+} ($3d_{5/2}$)/Mo^{4+}($3d_{3/2}$) (Table 1). The Mo^{6+}/Mo^{4+} ratio is determined to be 4.0 according to the line fitting results, hence the valence state of molybdenum on the surface of MMO can be determined as 5.6[18,20].

To further investigate the overall valence state of the MMO, TGA-DSC test was carried out to monitor the weight changes as a function of temperature in the air atmosphere and the results are shown in Fig. 4. The small weight loss (about 0.3%) at the temperature lower than 150 °C can be attributed to the loss of absorbed water. The

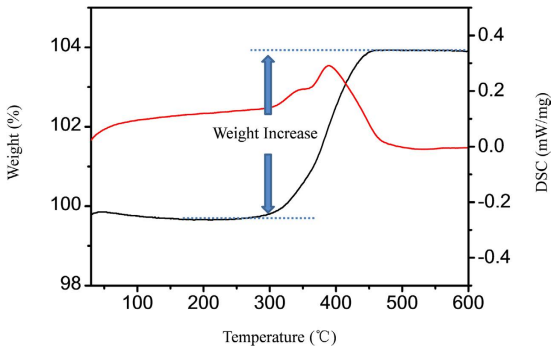

Figure 4. TGA-DSC curve of MMO in air at a heating rate of 5 °C/min.

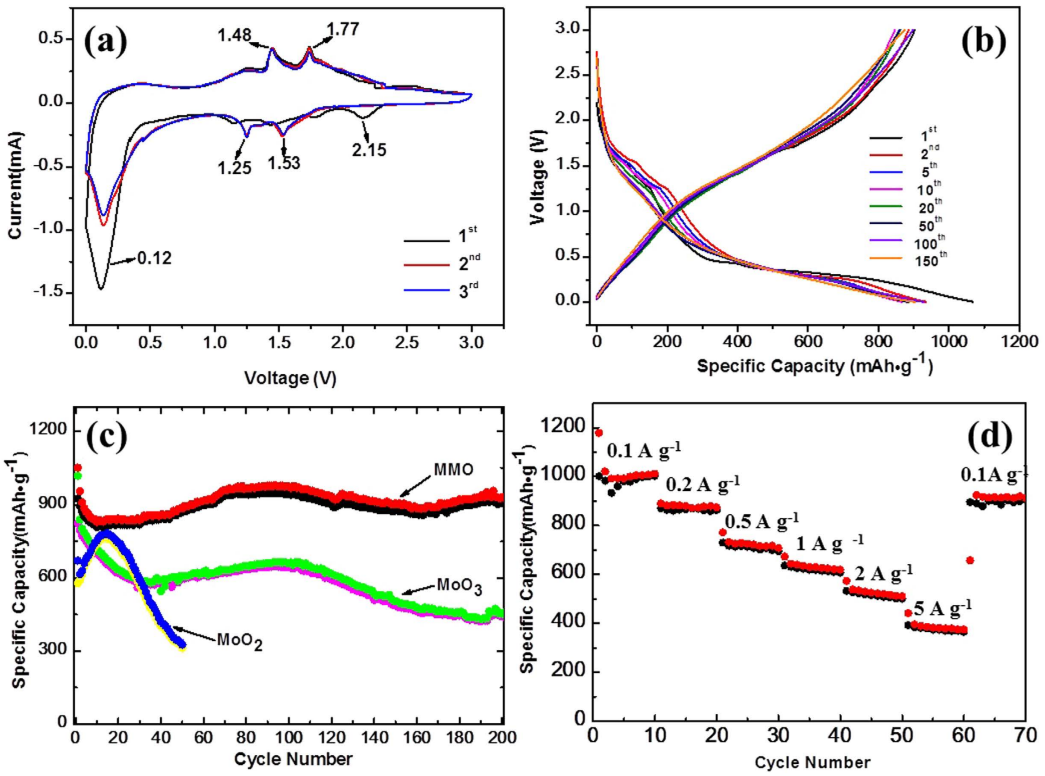

Figure 5. (**a**) Cyclic voltammograms of MMO at a scan rate of 0.2 mV·s^{-1} with a mass of 2.5 mg. (**b**) Discharge and charge curves of MMO at a current of 100 mA·g^{-1} in the potential window of 3–5 × 10^{-3} V vs. Li^{+}/Li. (**c**) The specific discharge/charge capacity vs cycle number plots for different samples at a current of 200 mA·g^{-1}. (**d**) Specific capacity vs cycle number curves at different current densities.

weight increase at 300–500 °C corresponds to the oxidization of MMO (MoO_x) to MoO_3 in the air and a wide exothermic peak is associated with this process. The total weight increase is 4.30% (Fig. 4), and thus x in MoO_x can be extracted as 2.63, leading to a calculated average valence state of 5.26 for all Mo ions in the sample MMO. This value determined by TGA is apparently lower than the valence state of surface Mo ions determined by XPS, indicating that the surface of MMO was oxidized to a higher extent compared to the inner part of the material. On the basis of the nominal formula of $MoO_{2.63}$ the theoretical capacity of MMO is 1021 mAh·g^{-1} based on the conversion mechanism.

Cyclic voltammetry (CV) was used to study the Li insertion/extraction behaviors in different samples and the results are presented in Fig. 5a. The redox peaks centered at 1.25/1.53 V and 1.48/1.77 V are attributed to the reversible monoclinic–orthorhombic–monoclinic phase transitions in the partially lithiated Li_xMoO_2 according to the CV data of MoO_2 nanoparticles (Figure s1a) and previous reports[6,19,21], consistent with the presence of MoO_2 in MMO which was illustrated in the XRD pattern and the TG curve[6,21]. Besides these two redox pairs, the whole CV curve of MMO is similar to that of our MoO_3 nanoparticles (Figure s1b) and literature[22–24] due to the high concentration of MoO_3, as implied by XRD and XPS data[22]. There are also intense peaks below 0.5 V, which can be associated with a conversion reaction with lithium, where Mo oxides are reduced completely to metallic

Mo along with the formation of Li_2O. The curve changes very little in the following cycles, suggesting that the partially lithiated Li_xMoO_2 structure is very stable during the charge-discharge progress, thus MMO is expected to have a good cycling performance[25]. Meanwhile the difference between the first and following cycles can be attributed to irreversible reactions such as the irreversible phase transition, the decomposition of the electrolyte and the formation of a solid electrolyte interface (SEI) layer[22,26].

To further investigate the electrochemical performance of the samples, galvanostatic experiments were performed on the coin cells. Figure 5b shows the charge/discharge plots of MMO at a current of 200 $mA{\cdot}g^{-1}$. The initial discharge capacity is 1068.2 $mAh{\cdot}g^{-1}$, slightly higher than the theoretical capacity of MMO (1021 $mAh{\cdot}g^{-1}$), which can be assigned to some irreversible reactions, e.g. the generation of an SEI layer[23,27]. In agreement with the CV results, two short discharge plateaus at about 1.55 and 1.26 V can be observed[13,21]. The expected charge plateaus at around 1.4 and 1.7 V are not clearly visible, which is similar to previously reported MoO_3 nanostructures[26]. The charge/discharge curves are very stable with continued cycling, suggesting good cycling performances, except that the voltage of discharge plateaus decreases and eventually the plateau can no longer be observed. Since the plateaus are usually attributed to the phase transition in the partially lithiated Li_xMoO_2, the decrease in voltage can be ascribed to the transformation of crystalline phase to amorphous-like structure[13,21].

As shown in Fig. 5c, the electrochemical performance of MMO is much better than MoO_2 or MoO_3. For MoO_2, the first discharge capacity is only 670.5 $mAh{\cdot}g^{-1}$ while the capacity gradually increases upon cycling and attains 781.7 $mAh{\cdot}g^{-1}$ after 15 cycles. This activation process has been reported by other groups and may be attributed to the partial loss of crystallinity of the material during the cycling[13,28,29], accompanied with a larger fraction of the material undergoing further conversion reaction instead of stopping at Li_xMoO_2 phase[30]. Nonetheless, a rapid capacity deterioration decay can be observed once the capacity reaches the maximum value and only a capacity of 325.7 $mAh{\cdot}g^{-1}$ remains after 50 cycles. The initial capacity of MoO_3 is 1017.6 $mAh{\cdot}g^{-1}$, however, it drops to 593.4 $mAh{\cdot}g^{-1}$ after only 30 cycles due to the big volume changes during cycling. Such decrease can also be observed in MMO, which has a large fraction of MoO_3. However, the drop in capacity is much less. The capacity decreases from the first discharge capacity of 1068.2 $mAh{\cdot}g^{-1}$ to 842.3 $mAh{\cdot}g^{-1}$ after 20 cycles, corresponding to a capacity loss of 12% (calculated based on the capacity of 2^{nd} and 20^{th} cycles). After that, the capacity increases slowly and reaches 976.3 $mAh{\cdot}g^{-1}$ after 90 cycles. The discharge capacity of the MMO only decreases slightly to 930.6 $mAh{\cdot}g^{-1}$ after 200 cycles, which is equivalent to a capacity retention of 95% of the maximum value of 977 $mAh{\cdot}g^{-1}$, demonstrating high capacity and excellent stability. Such high reversible capacity of more than 930.6 $mAh{\cdot}g^{-1}$ at 200 $mA{\cdot}g^{-1}$ is almost three-fold that of commercial graphite (~330 $mAh{\cdot}g^{-1}$). Although the overall profile of MMO's cycling curve is similar to that of MoO_3, the key difference is the capacity decay is much smaller for MMO than MoO_3. This decay, which can be seen in many reports of MoO_3, is generally assigned to the huge volume and/or structure change during the conversion reaction[23,27]. Since the volume and structure changes are very limited in the insertion reaction[31], the presence of stable partially lithiated Li_xMoO_2 in MMO is expected to help stabilize the whole electrode and avoid the capacity loss. To further investigate the hypothesis above, the electrochemical performance of the mixed MoO_2 and MoO_3 sample was prepared by ball milling (MMM) (Figure S2b). Although MMM is also composed of MoO_2 and MoO_3 with similar proportion (Figure S2a), the electrochemical performance is apparently worse than that of MMO. Although an initial capacity of 1050 $mAh{\cdot}g^{-1}$ can be obtained, which is similar to that of MMO, only a capacity of approximately 100 $mAh{\cdot}g^{-1}$ can retain after 100 cycles at a current rate of 200 $mA{\cdot}g^{-1}$. The very rapid decay can be ascribed to the phase isolation which is expected to accelerate the pulverization process. Owing to the poor electrochemical performances of Mo_4O_{11}[32], which is the intermediate phase in the transformation from MoO_2 to MoO_3[33], the small fraction of Mo_4O_{11} in MMO is also unlikely to be associated with the improved electrochemical properties.

The rate capability of MMO was further investigated and the results are shown in Fig. 5d. The material was tested with the potential range of 5×10^{-3}–3.0 V at 0.1 $A{\cdot}g^{-1}$, 0.2 $A{\cdot}g^{-1}$, 0.5 $A{\cdot}g^{-1}$, 1 $A{\cdot}g^{-1}$, 2 $A{\cdot}g^{-1}$, 5 $A{\cdot}g^{-1}$ and 0.1 $A{\cdot}g^{-1}$ for 10 cycles each. The specific capacity reaches 994 $mAh{\cdot}g^{-1}$ at 0.1 $A{\cdot}g^{-1}$, 883 $mAh{\cdot}g^{-1}$ at 0.2 $A{\cdot}g^{-1}$, 735 $mAh{\cdot}g^{-1}$ at 0.5 $A{\cdot}g^{-1}$, 644 $mAh{\cdot}g^{-1}$ at 1 $A{\cdot}g^{-1}$, 538 $mAh{\cdot}g^{-1}$ at 2 $A{\cdot}g^{-1}$, 397 $mAh{\cdot}g^{-1}$ at 5 $A{\cdot}g^{-1}$, respectively. A specific capacity of 397 $mAh{\cdot}g^{-1}$ at 5 $A{\cdot}g^{-1}$ for this material is as high as 40% of its capacity at 0.1 $A{\cdot}g^{-1}$ (994 $mAh{\cdot}g^{-1}$). The results show that MMO has a better rate capability compared to previous reports[26,34] It is noteworthy that this high performance is achieved without coating the active material with carbon based conductors such as graphene.

Table 2 summarizes some recent works on molybdenum oxide based materials as anodes for lithium ion batteries. The specific capacity (930.6 mAh g^{-1}, 0.2 $A{\cdot}g^{-1}$) and cycling performance of MMO in this work excels most of the molybdenum oxide based materials previously reported in the literature, and even those with carbon coating[35–41].

To further understand lithium storage mechanisms of MMO, Solid-State NMR and XRD experiments on lithiated samples were performed. ^{7}Li NMR spectroscopy proves to be a powerful method to investigate the relationship between local structures and electrochemical performances of materials for lithium ion batteries and to reveal the electrochemical reaction mechanisms[42]. ^{7}Li MAS NMR spectra of the MMO and MoO_3 lithiated to 5×10^{-3} V are given in Fig. 6. A broad resonance can be seen at 2.6 ppm in the spectrum of lithiated MoO_3, which can be attributed to Li_2O which is the product of the conversion reaction. The resonance of the lithiated oxide is broader compared to the spectrum of commercial Li_2O standard sample, indicating more complex local structures of the lithium ions after the lithiation process, and/or the magnetic fields generated by the Mo particles[22]. Similarly, the broad peak at 2.6 ppm in the spectrum of lithiated MMO can be assigned to Li_2O formed in the conversion reaction. A sharp peak at −7.0 ppm can also be observed for MMO, indicating that there is another local environment of lithium ions.

The presence of the other lithium compound is further supported by XRD data of lithiated MMO (Fig. 7). The Kapton film was used to protect the air-sensitive fully lithiated sample and its broad background peak can be

Materials	Capacity (mAh g^{-1})	Current Density (A g^{-1})	Cycle number	Year	Ref.
a-MoO_2 particles	910	0.1	50	2012	35
a-MoO_x-C microballs	733	2	300	2013	36
F-doped a-MoO_x	905	0.2	50	2014	37
MoS_2/MoO_2 nanonetworks	1025	0.2	80	2014	38
MoO_{3-x}/CNT	421	0.2	100	2014	39
MoO_2/Mo_2C heteronanotubes	790	0.2	140	2014	41
Standing carbon-coated MoO_2 nanosheets ongraphene	587	1	200	2015	40
MMO	930.6	0.2	200	This Work	

Table 2. Comparison of the capacity of MMO in this work with those of other recently reported molybdenum oxide based materials as anodes for LIBs.

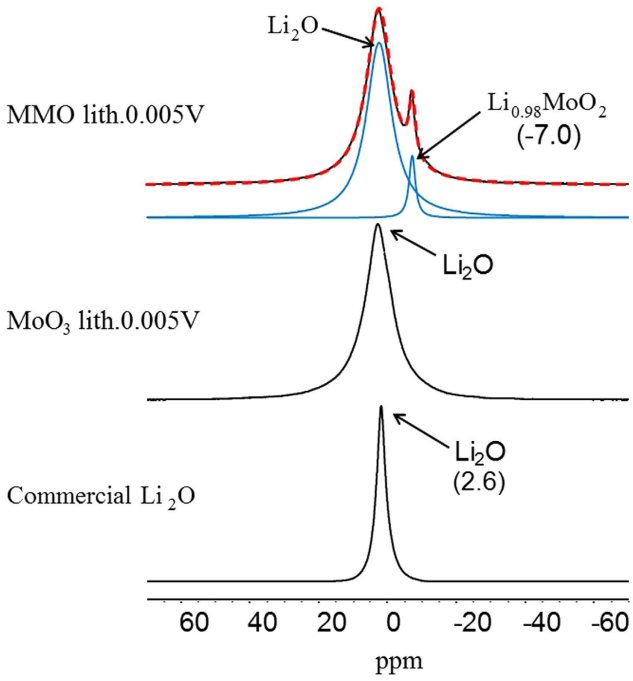

Figure 6. ^{7}Li solid-state NMR spectra of MMO lithiated to 5×10^{-3} V with a simulation (dashed line in red) fitted with each individual component (solid lines in blue), in comparison to MoO3 lithiated to 5×10^{-3} V and commercial Li2O, for comparison. Spinning rate: 20 kHz.

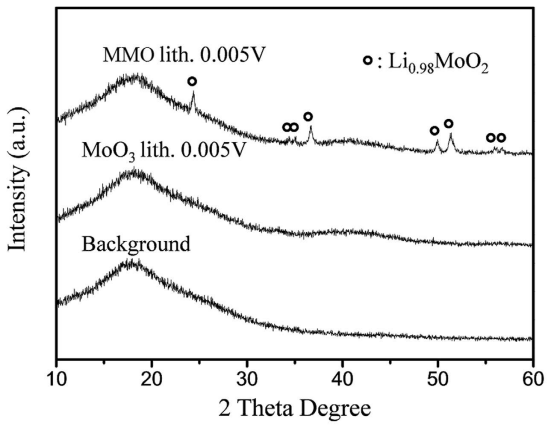

Figure 7. XRD patterns of MMO and MoO_3 after lithiated to 5×10^{-3} V with the protection of Kapton film, in comparison with the background.

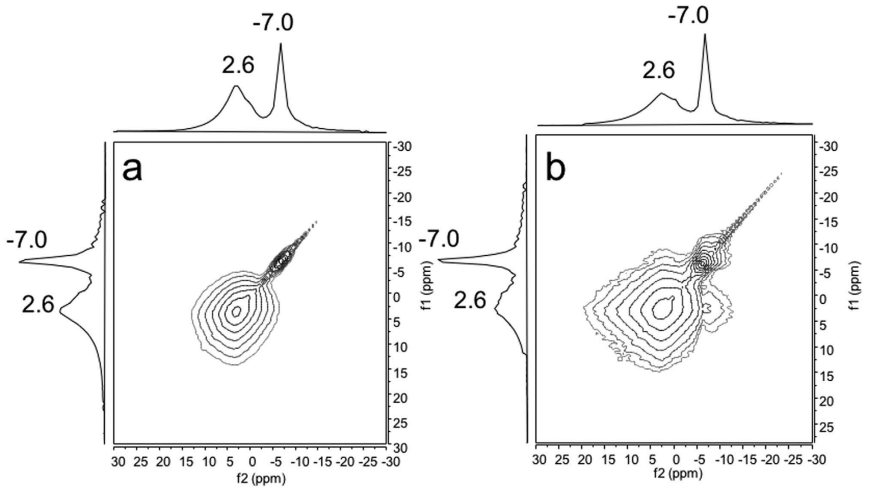

Figure 8. ^{7}Li 2D-exchange NMR spectra of MMO lithiated to 5×10^{-3} V with (**a**) (mixing time = 1 μs) and (**b**) (mixing time = 100 ms). Spinning rate: 20 kHz.

found between 2θ of 10–30°. No distinct peaks can be seen in the pattern of lithiated MoO_3, suggesting the poor crystallinity of the product after lithiation. However, pronounced peaks due to $Li_{0.98}MoO_2$, which was previously reported as the product of the insertion reaction of MoO_2[30], appear in the pattern of lithiated MMO. In combination with the results of ^{7}Li MAS NMR spectra of MMO after lithiation, it is clear that two mechanisms including both conversion and insertion reactions are involved in the lithiation of MMO (MoOx) while only conversion reaction is associated with MoO_3. Assuming MoO_3 in MMO only undergoes a conversion reaction while MoO_2 is associated with both insertion/extraction and conversion reaction, the fraction of MoO_2 (x) which underwent insertion/extraction reaction in MMO can be estimated in the following equation (considering the theoretical capacity of MoO_2 with insertion/extraction mechanism is 210 mAh/g):

$$C_{i/e}(MoO_2,\ 210\,mAh/g) \times x + C_c(MoO_2,\ 838\,mAh/g) \times (0.37 - x) + C_c(MoO_3,\ 1117\,mAh/g) \times 0.63 = 977\,mAh/g$$

(the charge capacity of the 1st cycle)

Thus, the value of x can be determined as 0.058, implying 16% of the MoO_2 material underwent the insertion/extraction reaction in the MMO material. The capacity of MMO increased after 50 cycles, indicating that more MoO_2 underwent conversion reaction[20,30]. This activation process, which has been reported many times, can be ascribed to the transformation from insertion reaction to conversion reaction, corresponding to the slowly decreasing of discharge plateaus at about 1.5 V[21].

Two-dimensional exchange (EXSY) ^{7}Li spectra provides more detailed information on the structure of MMO and additional evidences for its better electrochemical properties[43,44]. With a short mixing time of 1 μs, only two peaks on the diagonal at (2.6, 2.6) and (−7.0, −7.0) corresponding to Li_2O and $Li_{0.98}MoO_2$ can be observed in the 2D EXSY spectrum (Fig. 8a). However, small cross peaks at (2.6, −7.0) and (−7.0, 2.6) can be observed at a much longer mixing time of 100 ms for MMO (Fig. 8b) while no peak is present at the same mixing time for MMM (Figure S3). It suggests that the two species in MMO are close in proximity and this mixing time is long enough for chemical exchange processes to occur in which lithium ions move across the interfaces between the two sites. The conclusion that the insertion and conversion reaction products $Li_{0.98}MoO_2$ and Li_2O are close in space implies that MoO_2 and MoO_3 regions are well mixed at the microscale in MMO, while this is not the situation in the sample MMM. The much lower capacity in MMM is presumably associated with the large volume change of MoO_3 (104% volume change) during cycling[27,45] and the resulting aggregation and/or sluggish kinetics of lithium ion insertion for the MoO_2 nanoparticles[28,29]. Since the MoO_2 and MoO_3 species are not well mixed at the microscale for MMM, inhomogeneous distribution causes phase isolation during cycling, which will lead to pulverization and rapid capacity decay. It has been demonstrated that superior stability can be achieved for the sample with a closer combination between mixed valence lithium vanadates formed in an *in-situ* transformation than other common coating methods[14,46]. The boost of the electrical performances may be explained as the results of synergistic interactions[34,47–50]. Since transformation from MoO_2 to $Li_{0.98}MoO_2$ in insertion reaction only involves small volume/structure change in the very initial cycles, the well dispersed MoO_2 helps to keep the integrity of the electrode and prevent the loss of active materials.

Although it is common that only insertion reaction occurs for bulk MoO_2, nanostructured MoO_2 often undergoes conversion reaction in further lithiation, presumably due to faster kinetics[30]. According to the XRD and NMR results of lithiation samples of MoO_2 (Figure S4), the intermediate phase $Li_{0.98}MoO_2$ still exist after 5 cycles, which helps stabilize the structure[44]. The much more stable $Li_{0.98}MoO_2$ in the lithiated MMO nanoparticles may be attributed to the high concentraion of MoO_3 around MoO_2 in MMO. MoO_3 is associated with a higher equilibrium potential and a lower activation barrier compared to MoO_2, thus conversion reaction will be easier to

occur during lithiation[26]. The generated amorphous Mo and Li_2O have poor electronic conductivity and ionic conductivity, therefore slowing down the kinetics and making further lithiation of $Li_{0.98}MoO_2$ more difficult[26,30].

Conclusion

In conclusion, MMO is developed from the moderately oxidization reaction of molybdenum dioxide nanoparticles. The nominal composition of the material can be calculated as $MoO_{2.63}$, according to the TGA results. MMO shows a high cyclability of 930.6 $mAh \cdot g^{-1}$ after 200 cycles at a current of 200 $mA \cdot g^{-1}$ as the anode material for lithium ion batteries. The formation of stable $Li_{0.98}MoO_2$ in the lithiation of MMO is confirmed with NMR and XRD on lithiated sample. 2D NMR results confirm that MoO_2 and MoO_3 are well mixed at the microscale. Both insertion/extraction and conversion reaction mechanisms are involved and the fraction of MoO_2 which undergoes the former reactions is estimated to be 16%. The insertion/extraction process stabilizes the electrode material and decrease the volume change generated from conversion reaction of MoO_3. This synergistic interaction is believed to be the key to the excellent electrochemical performances and this approach can be applied in many other transition metal oxides to provide advanced electrode materials.

References

1. Armand, M. & Tarascon, J.-M. Building better batteries. *Nature* **451,** 652–657 (2008).
2. Cao, X. *et al.* Preparation of MoS_2-Coated Three-Dimensional Graphene Networks for High-Performance Anode Material in Lithium-Ion Batteries. *Small* **9,** 3433–3438 (2013).
3. Goodenough, J. B. & Kim, Y. Challenges for Rechargeable Li Batteries†. *Chem. Mater.* **22,** 587–603 (2009).
4. Reddy, M., Subba Rao, G. & Chowdari, B. Metal oxides and oxysalts as anode materials for Li ion batteries. *Chem. Rev.* **113,** 5364–5457 (2013).
5. Zhang, H.-J. *et al.* Uniform hierarchical MoO_2/carbon spheres with high cycling performance for lithium ion batteries. *Journal of Materials Chemistry A* **1,** 12038 (2013).
6. Wang, Z., Chen, J. S., Zhu, T., Madhavi, S. & Lou, X. W. One-pot synthesis of uniform carbon-coated MoO_2 nanospheres for high-rate reversible lithium storage. *Chemical Communications* **46,** 6906–6908 (2010).
7. Koziej, D. *et al.* Interplay Between Size and Crystal Structure of Molybdenum Dioxide Nanoparticles—Synthesis, Growth Mechanism, and Electrochemical Performance. *Small* **7,** 377–387 (2011).
8. Chen, J. S. & Lou, X. W. SnO_2-Based Nanomaterials: Synthesis and Application in Lithium-Ion Batteries. *Small* **9,** 1877–1893 (2013).
9. Xia, X. *et al.* Oxide Nanostructures Hyperbranched with Thin and Hollow Metal Shells for High-Performance Nanostructured Battery Electrodes. *Small* **10,** 2419–2428 (2014).
10. Ma, F., Yuan, A., Xu, J. & Hu, P. Porous α-MoO_3/MWCNT Nanocomposite Synthesized via a Surfactant-Assisted Solvothermal Route as a Lithium-Ion-Battery High-Capacity Anode Material with Excellent Rate Capability and Cyclability. *ACS Appl. Mater. Interfaces* 7, 15531–15541 (2015).
11. Ahmed, B. *et al.* Surface Passivation of MoO_3 Nanorods by Atomic Layer Deposition toward High Rate Durable Li Ion Battery Anodes. *ACS Appl. Mater. Interfaces* 7, 13154–13163 (2015).
12. Zhang, X. *et al.* Facile synthesis of yolk–shell MoO_2 microspheres with excellent electrochemical performance as a Li-ion battery anode. *Journal of Materials Chemistry A* **1,** 6858 (2013).
13. Liu, J. *et al.* Synthesis of Mo_2N nanolayer coated MoO_2 hollow nanostructures as high-performance anode materials for lithium-ion batteries. *Energy & Environmental Science* **6** (2013).
14. Sun, D. *et al.* $LixV_2O_5$/LiV_3O_8 nanoflakes with significantly improved electrochemical performance for Li-ion batteries. *J. Mater. Chem. A* **2,** 8009–8016 (2014).
15. Liu, Y., Zhang, H., Ouyang, P. & Li, Z. One-pot hydrothermal synthesized MoO_2 with high reversible capacity for anode application in lithium ion battery. *Electrochim. Acta* **102,** 429–435 (2013).
16. Liu, T. *et al.* Cycling Li-O_2 batteries via LiOH formation and decomposition. *Science* **350,** 530–533 (2015).
17. Yang, L., Gao, Q., Tang, Y., Wu, Y. & Holze, R. MoO_2 synthesized by reduction of MoO_3 with ethanol vapor as an anode material with good rate capability for the lithium ion battery. *J. Power Sources* **179,** 357–360 (2008).
18. Chen, W., Zhang, H., Wang, Y., Ma, Z. & Li, Z. *In-situ* Microstructural Investigations by Electron-beam Irradiation Induced Crystallization of Amorphous MoO_x Thin Films with High Performance for Li-ion Storage. *Electrochim. Acta* **144,** 369–375 (2014).
19. Sen, U. K., Shaligram, A. & Mitra, S. Intercalation anode material for lithium ion battery based on molybdenum dioxide. *ACS Appl Mater Interfaces* **6,** 14311–14319 (2014).
20. Liu, Y. *et al.* High electrochemical performance and phase evolution of magnetron sputtered MoO_2 thin films with hierarchical structure for Li-ion battery electrodes. *Journal of Materials Chemistry A* **2,** 4714 (2014).
21. Guo, B. *et al.* Synthesis and Lithium Storage Mechanism of Ultrafine MoO_2Nanorods. *Chem. Mater.* **24,** 457–463 (2012).
22. Ji, W. *et al.* Partially nitrided molybdenum trioxide with promoted performance as an anode material for lithium-ion batteries. *Journal of Materials Chemistry A* **2,** 699 (2014).
23. Zhao, G., Zhang, N. & Sun, K. Electrochemical preparation of porous MoO_3 film with a high rate performance as anode for lithium ion batteries. *Journal of Materials Chemistry A* **1,** 221 (2013).
24. Dedryvere, R. *et al.* Contribution of X-ray photoelectron spectroscopy to the study of the electrochemical reactivity of CoO toward lithium. *Chemistry of materials* **16,** 1056–1061 (2004).
25. Bhaskar, A., Deepa, M. & Narasinga Rao, T. MoO_2/multiwalled carbon nanotubes (MWCNT) hybrid for use as a Li-ion battery anode. *ACS Appl Mater Interfaces* **5,** 2555–2566 (2013).
26. Wang, Z., Madhavi, S. & Lou, X. W. Ultralong α-MoO_3 Nanobelts: Synthesis and Effect of Binder Choice on Their Lithium Storage Properties. *J. Phys. Chem. C* **116,** 12508–12513 (2012).
27. Tao, T. *et al.* MoO_3 nanoparticles dispersed uniformly in carbon matrix: a high capacity composite anode for Li-ion batteries. *J. Mater. Chem.* **21,** 9350 (2011).
28. Sun, Y., Hu, X., Luo, W. & Huang, Y. Self-assembled hierarchical MoO_2/graphene nanoarchitectures and their application as a high-performance anode material for lithium-ion batteries. *ACS nano* **5,** 7100–7107 (2011).
29. Ihsan, M. *et al.* MoO_2/Mo_2C/C spheres as anode materials for lithium ion batteries. *Carbon* **96,** 1200–1207 (2016).
30. Ku, J. H., Jung, Y. S., Lee, K. T., Kim, C. H. & Oh, S. M. Thermoelectrochemically Activated MoO_2 Powder Electrode for Lithium Secondary Batteries. *J. Electrochem. Soc.* **156,** A688 (2009).
31. Lazzari, M. & Scrosati, B. A cyclable lithium organic electrolyte cell based on two intercalation electrodes. *J. Electrochem. Soc.* **127,** 773–774 (1980).
32. Shembel, E. *et al.* Electrolytic molybdenum oxides in lithium batteries. *J. Solid State Electrochem.* **9,** 96–105 (2005).
33. Dieterle, M. & Mestl, G. Raman spectroscopy of molybdenum oxides Part II. Resonance Raman spectroscopic characterization of the molybdenum oxides Mo_4O_{11} and MoO_2. *Phys. Chem. Chem. Phys.* **4,** 822–826 (2002).
34. Deng, Z. *et al.* Reciprocal hybridization of MoO_2 nanoparticles and few-layer MoS_2 for stable lithium-ion batteries. *Chem. Commun.* **51,** 13838–13841 (2015).

35. Ku, J. H., Ryu, J. H., Kim, S. H., Han, O. H. & Oh, S. M. Reversible Lithium Storage with High Mobility at Structural Defects in Amorphous Molybdenum Dioxide Electrode. *Adv. Funct. Mater.* **22,** 3658–3664 (2012).
36. Teh, P. F., Sharma, Y., Ko, Y. W., Pramana, S. S. & Srinivasan, M. Tuning the morphology of $ZnMn_2O_4$ lithium ion battery anodes by electrospinning and its effect on electrochemical performance. *RSC Adv.* **3,** 2812–2821 (2013).
37. Liu, B., Zhao, X., Xiao, Y. & Cao, M. High-surface-area F-doped amorphous MoOx with high-performance lithium storage properties. *Journal of Materials Chemistry A* **2,** 3338–3343 (2014).
38. Xu, Z. *et al.* Sulfur Refines MoO_2 Distribution Enabling Improved Lithium Ion Battery Performance. *J. Phys. Chem. C* **118,** 18387–18396 (2014).
39. Ni, J. F. *et al.* Carbon nanotube-wired and oxygen-deficient MoO_3 nanobelts with enhanced lithium-storage capability. *J. Power Sources* **247,** 90–94 (2014).
40. Guo, L. & Wang, Y. Standing carbon-coated molybdenum dioxide nanosheets on graphene: morphology evolution and lithium ion storage properties. *Journal of Materials Chemistry A* **3,** 4706–4715 (2015).
41. Zhang, H.-J. *et al.* MoO_2/Mo_2C Heteronanotubes Function as High-Performance Li-Ion Battery Electrode. *Adv. Funct. Mater.* **24,** 3399–3404 (2014).
42. Grey, C. P. & Dupré, N. NMR studies of cathode materials for lithium-ion rechargeable batteries. *Chem. Rev.* **104,** 4493–4512 (2004).
43. Ellis, B. L., Ramesh, T., Davis, L. J., Goward, G. R. & Nazar, L. F. Structure and electrochemistry of two-electron redox couples in lithium metal fluorophosphates based on the tavorite structure. *Chem. Mater.* **23,** 5138–5148 (2011).
44. Harris, K. J. *et al.* Electrochemical Changes in Lithium-Battery Electrodes Studied Using ^{7}Li NMR and Enhanced ^{13}C NMR of Graphene and Graphitic Carbons. *Chem. Mater.* **27,** 3299–3305 (2015).
45. Jung, Y. S., Lee, S., Ahn, D., Dillon, A. C. & Lee, S.-H. Electrochemical reactivity of ball-milled MoO_{3-y} as anode materials for lithium-ion batteries. *J. Power Sources* **188,** 286–291 (2009).
46. Wang, H. *et al.* AlF3 coated LiV_3O_8 nanosheets with significantly improved cycling stability as cathode material for Li-ion battery. *Solid State Ionics* **236,** 37–42 (2013).
47. Wang, L. *et al.* Mesostructural Bi-Mo-O catalyst: correct structure leading to high performance. *Sci. Rep.* **3,** 6 (2013).
48. Zhao, Y. *et al.* Stable Alkali Metal Ion Intercalation Compounds as Optimized Metal Oxide Nanowire Cathodes for Lithium Batteries. *Nano Lett.* **15,** 2180–2185 (2015).
49. Luo, Y. *et al.* Seed-assisted synthesis of highly ordered TiO_2@α-Fe_2O_3 core/shell arrays on carbon textiles for lithium-ion battery applications. *Energy & Environmental Science* **5,** 6559 (2012).
50. Gao, L., Hu, H., Li, G., Zhu, Q. & Yu, Y. Hierarchical 3D TiO_2@Fe_2O_3 nanoframework arrays as high-performance anode materials. *Nanoscale* **6,** 6463–6467 (2014).

Acknowledgements

This work is supported by National Basic Research Program of China (2013CB934800), National Natural Science Foundation of China (NSFC) (21573103, 21222302 and 20903056), NSFC-Royal Society Joint Program (21661130149 and 21111130201), Program for New Century Excellent Talents in University (NCET-10-0483), the Fundamental Research Funds for the Central Universities (1124020512) and National Science Fund for Talent Training in Basic Science (J1103310). L.P. thanks Royal Society and Newton Fund for Royal Society - Newton Advanced Fellowship. This work was also supported by a Project Funded by the Priority Academic Program Development of Jiangsu Higher Education Institutions.

Author Contributions

L.P., W.D. and M.J. contributed to the conception and design of the experiment, analysis of the data and writing the manuscript. D.W. and R.S. carried out design, synthesis and characterization of the materials. D.W. carried out the measurement of solid state NMR and corresponding writing. R.Y. and W.J. carried out the measurement of electrochemical performance. All the authors contributed to discussion on the results and preparation of manuscript. All authors have given approval to the final version of the manuscript.

Additional Information

Supplementary information accompanies this paper at http://www.nature.com/srep

Competing Interests: The authors declare no competing financial interests.

How to cite this article: Wu, D. *et al.* Mixed Molybdenum Oxides with Superior Performances as an Advanced Anode Material for Lithium-Ion Batteries. *Sci. Rep.* **7**, 44697; doi: 10.1038/srep44697 (2017).

Publisher's note: Springer Nature remains neutral with regard to jurisdictional claims in published maps and institutional affiliations.